

Lawrence Berkeley National Laboratory

LBL Publications

Title

Low Noise Frequency-Domain Multiplexing of TES Bolometers Using SQUIDs at Sub-Kelvin Temperature

Permalink

<https://escholarship.org/uc/item/6z50j6xc>

Journal

Journal of Low Temperature Physics, 209(3-4)

ISSN

0022-2291

Authors

Elleflot, T
Suzuki, A
Arnold, K
[et al.](#)

Publication Date

2022-11-01

DOI

10.1007/s10909-022-02796-8

Copyright Information

This work is made available under the terms of a Creative Commons Attribution License, available at <https://creativecommons.org/licenses/by/4.0/>

Peer reviewed



Low Noise Frequency-Domain Multiplexing of TES Bolometers Using SQUIDs at Sub-Kelvin Temperature

T. Elleflot¹ · A. Suzuki¹ · K. Arnold² · C. Bebek¹ · R. H. Cantor³ · K. T. Crowley⁴ · J. Groh⁵ · T. de Haan⁶ · A. Hornsby⁴ · J. Joseph¹ · A. T. Lee^{1,4} · T. Liu⁷ · J. Montgomery⁸ · M. Russell² · Q. Yu⁴

Received: 1 November 2021 / Accepted: 15 April 2022 / Published online: 7 October 2022
© The Author(s) 2022

Abstract

Digital Frequency-Domain Multiplexing (DfMux) is a technique that uses MHz superconducting resonators and Superconducting Quantum Interference Device (SQUID) arrays to read out sets of transition edge sensors. DfMux has been used by several Cosmic Microwave Background experiments, including most recently POLARBEAR-2 and SPT-3 G with multiplexing factors as high as 68, and is the baseline readout technology for the planned satellite mission *LiteBIRD*. Here, we present recent work focused on improving DfMux readout noise, reducing parasitic impedance, and improving sensor operation. We have achieved a substantial reduction in stray impedance by integrating the sensors, resonators, and SQUID array onto a single-carrier board operated at 250 mK. This also drastically simplifies the packaging of the cryogenic components and leads to better-controlled crosstalk. We demonstrate a low readout noise level of $8.6 \text{ pA/Hz}^{1/2}$, which was made possible by operating the SQUID array at a reduced temperature and with a low dynamic impedance. This is a factor of two improvement compared to the achieved readout noise level in currently operating Cosmic Microwave Background experiments using DfMux and represents a critical step toward maturation of the technology for the next generation of instruments.

Keywords Frequency-domain multiplexing · Transition edge sensors · Readout electronics · Cosmic Microwave Background

✉ T. Elleflot
tuckerelleflot@gmail.com

Extended author information available on the last page of the article

1 Introduction

Digital Frequency-Domain Multiplexing (DfMux) [1–3] is a TES multiplexing technique, in which sets of $\sim 1 \Omega$ TES bolometers are placed in series with superconducting LC resonators [4] that define unique $\mathcal{O}(1)$ MHz bias frequencies. A voltage bias is applied to each detector at the resonance frequency of its associated LC resonator, and the resulting current is actively nulled. Residual current is amplified by a cryogenic DC SQUID array and room temperature electronics and used to rapidly update the nulling current [5]. DfMux has been deployed in many Cosmic Microwave Background (CMB) experiments, including most recently POLARBEAR-2 and SPT-3 G with multiplexing factors as high as 68 [6]. DfMux is also the baseline readout technology for the planned CMB satellite mission *LiteBIRD* [7].

Here, we present recent work aimed at reducing readout noise and parasitic impedance and improving readout packaging [8, 9]. In section 2, we describe the hardware used for these measurements, including a technology demonstrator circuit board called the Cold Integrated Multiplexing Module (CIMM). The CIMM moves all cryogenic readout components onto a single circuit board that is cooled to 250 mK, reducing parasitic impedances that generate crosstalk and detector instability [1, 10, 11] and simplifying the readout packaging. In section 3, we present results from measurements performed using the CIMM, which include a factor of two reduction in readout noise and factor of five reduction in parasitic resistance compared to currently operating CMB DfMux systems. We conclude in Section 4.

2 Implementation

This work was done using a technology demonstrator circuit board called the CIMM, described previously in [8]. In contrast with deployed DfMux systems, in which the cryogenic readout components are spread across two cryogenic temperature stages [12], the CIMM holds all cryogenic readout components on a single printed circuit board at 250 mK. This dramatically reduces the parasitic impedance associated with the electrical connection between the SQUID and resonators, which is a source of crosstalk [1, 11], and relaxes the requirements on the $\mathcal{O}(1)$ m cable that spans the 4 K to 250 mK temperature differential, allowing us to use commercial twisted pair cable instead of the custom low-inductance cables used in deployed instruments.

Due to a subtlety of the SQUID feedback scheme used, the inductance of the SQUID array input coil and parasitic series inductance provide a mechanism for bias frequency-dependent readout noise [6, 11]. We designed the CIMM such that only on-chip impedances contribute to this effect (see Fig. 1). We chose to use an SA13ax SQUID array because of its low input inductance of 70 nH [13], high transimpedance, and variable dynamic impedance. The SA13ax is also used in the SPT-3 G and PB-2 receivers at a temperature of 4 K.

The CIMM also holds one LC resonator chip and up to five TES chips, allowing us to operate 40 detectors. The TES bias is provided by a 4.2-nH controlled

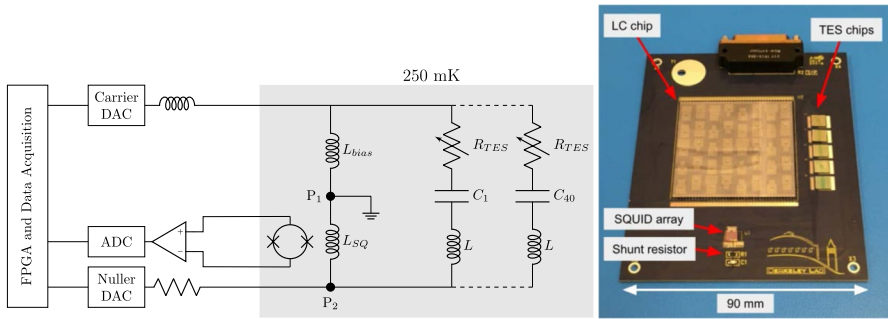


Fig. 1 (Color figure online) *Left*: Schematic of DfMux circuit with cryogenic components in gray shaded box. Inductance between points $P1$ and $P2$ is a source of bias frequency-dependent readout noise [6]. We minimize off-chip parasitic inductance by putting points $P1$ and $P2$ on the SQUID chip itself. *Right*: Photograph of CIMM printed circuit board with readout components labeled

inductance circuit board trace. The use of a reactive bias element reduces power dissipation on the sub-kelvin stage and provides a small reduction in readout noise. The use of a reactive TES bias element has been studied previously, e.g., [1, 8, 10, 14].

Magnetic shielding was provided by several layers of high magnetic permeability foil (Metglas 2705 M). Care was taken to ensure that no ferromagnetic materials were used in the fabrication of the circuit board. The assembly was installed on the sub-kelvin stage of a cryostat cooled with a pulse tube cryocooler and a helium adsorption cooler with a base temperature of 250 mK. The connection from the CIMM to the room temperature electronics is made with twisted pair cable.

3 Results

3.1 SQUID Performance

We measured flux modulation curves at several temperatures between 4 K and 250 mK. The modulation curves were smooth at 4 m, but irregularities were observed on the rising slope of the curve at temperatures of 800 mK and below. The irregularities limit our choice of bias point and are thought to be associated with excess SQUID noise. Others have demonstrated reduced SQUID noise by using an RC snubber in parallel with the SQUID input coil [15]. We found that shunting the input coil with a $5\ \Omega$ cryogenic resistor completely removed the irregularities at all accessible temperatures (see Fig. 2). The resistor and input inductance of the SQUID input coil form a low-pass filter. We chose the shunt resistance value such that the cutoff frequency of the filter is above our readout bandwidth. During CIMM operation, the shunt resistor is at a temperature of 250 mK and its Johnson noise makes a negligible contribution to the total readout noise.

SQUID tuning is the process by which a current and flux bias are applied to the SQUID in order to achieve an optimum between readout noise and SQUID linearity.

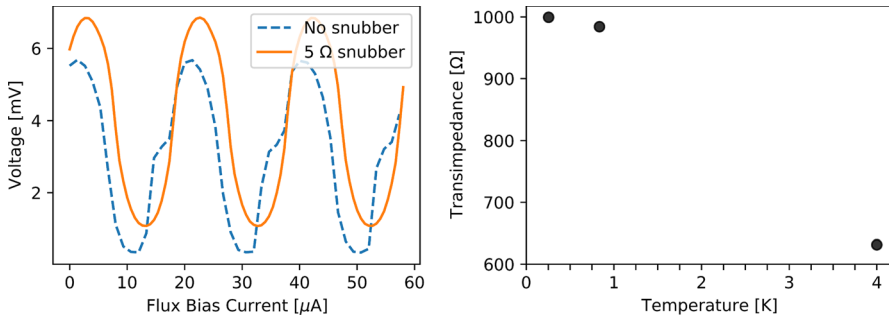


Fig. 2 (Color figure online) *Left:* The modulation curve for an SA13ax SQUID array measured at 250 mK with and without a 5 Ω shunt resistor in parallel with its input coil. *Right:* Transimpedance of an SA13ax SQUID array as a function of temperature. The array was tuned using an automated tuning algorithm that optimizes between Z_t and linearity

Tuning is usually performed using an automated routine, but can also be performed manually. After tuning, the transimpedance (Z_t) and dynamic impedance (R_{dyn}) of the array at the chosen bias point, defined below, can be measured [13, 16].

$$Z_t = \frac{\partial V}{\partial \Phi} M_{in} \quad (1)$$

$$R_{dyn} = \frac{\partial V}{\partial \Phi} \left(\frac{\partial I_{SQ}}{\partial \Phi} \right)^{-1} \quad (2)$$

In the equations above, V is the voltage across the SQUID, Φ is the magnetic flux applied to the SQUID, I_{SQ} is the SQUID bias current, and M_{in} is the mutual inductance of the SQUID and input coil.

We performed the automated SQUID tuning routine at several temperatures between 4 K and 250 mK and found that Z_t and R_{dyn} increased by 60% and 20%, respectively, over this temperature range. We also investigated the achievable range of Z_t and R_{dyn} values by manually tuning the SQUID to eleven different bias points while holding the CIMM at a constant temperature of 250 mK (Fig. 3). We observe a correlation between Z_t and R_{dyn} , which should be expected due to the common factor of $\frac{\partial V}{\partial \Phi}$ in their definitions. Using manual tuning, it is possible to increase Z_t by nearly a factor of two relative to the automated routine.

3.2 Readout Noise

Power absorbed by a bolometer is transduced into an amplitude modulation of the SQUID feedback current associated with the bolometer's bias frequency [5]. In the absence of signals and detector noise, we can take the demodulated signal as a measurement of readout noise. To perform this measurement, we replaced the TES sensors with 1 Ω resistors, which do not have a superconducting transition in the relevant temperature range and do not have sensitivity to optical power. The resistors

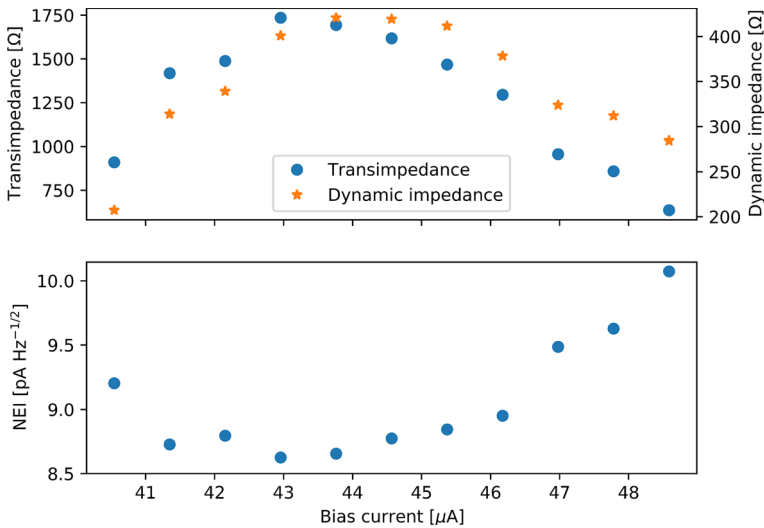


Fig. 3 (Color figure online) Measured values of Z_t and R_{dyn} (top) and readout noise (bottom) at 250 mK with several different values of current bias applied to the SQUID array

contribute Johnson noise to the measurement, which we conservatively estimated by assuming a low electron temperature of 250 mK and a resistance of 1Ω . This is removed when analyzing readout noise data, though it only accounts for about 10% of the total measured noise.

The SQUID dynamic impedance impacts readout noise in two ways: It converts the input current noise of the first-stage amplifier into a voltage noise at the output of the SQUID, and it forms a low-pass filter with the capacitance of the cryogenic wiring between the SQUID and 300 K amplifier [11]. For the SA13ax, $\frac{\partial I_{SQ}}{\partial \Phi}$ can take significantly different values on the positive and negative slopes of the modulation curve, resulting in R_{dyn} of $\sim 300 \Omega$ ($\sim 700 \Omega$) on the positive (negative) slope while maintaining a constant $Z_t \sim 1000 \Omega$. This allowed us to measure the impact of R_{dyn} on readout noise. We found that operating the SQUID with low R_{dyn} resulted in a reduction in readout noise of 6–8 $\text{pA}/\text{Hz}^{1/2}$ across the range of bias frequencies compared to operating with high R_{dyn} . This is consistent with our expectations based on the current noise of the room temperature amplifier. The latter effect was not expected to be important for this measurement because we are using a short length of cryogenic wiring with low-pass cutoff frequencies well above our readout bandwidth for both values of R_{dyn} , and indeed the invocation of this effect is not required to explain the measured readout noise.

Next, we studied the effect of SQUID tuning on readout noise (Fig. 3). We measured readout noise, while the CIMM was cooled to 250 mK for eleven different manual SQUID tunings. Despite the change in Z_t and R_{dyn} by a factor of about two over the range of current biases, we measure only a $\sim 10\%$ change in median readout noise. We previously described a correlation between R_{dyn} and readout noise, and this measurement implies an anti-correlation between Z_t and readout noise. Together, these observations are consistent with the dominant noise

source being the first-stage amplifier following the SQUID. The broad minimum in readout noise indicates that there is flexibility in optimizing SQUID linearity without significantly affecting readout noise performance. The lowest achieved median noise level is $8.6 \text{ pA/Hz}^{1/2}$. This represents a factor of two reductions in readout noise compared to currently observing CMB experiments using DfMux. The bias frequency dependence of the readout noise is also greatly suppressed (Fig. 4). We measure an increase in noise by about 15% at our highest bias frequencies, which should be compared to a $\sim 100\%$ increase in noise in deployed CMB DfMux systems.

We refer the measured readout noise to the input of a *LiteBIRD*-like bolometer by assuming a $1 \text{ } \Omega$ TES operating resistance and a conservative 1 pW electrical bias power [17]. In all observing bands, the measured readout noise is below the projected *LiteBIRD* sensitivity [18].

3.3 TES Operation

We verified TES operation by simultaneously lowering the voltage biases applied to a set of TES bolometers such that they cooled through their superconducting transitions. This was done by first heating the CIMM above the critical temperature of the sensors ($\sim 450 \text{ mK}$) and applying a large voltage bias of $\sim 10 \text{ } \mu\text{V}$ using the CIMM's inductive bias element. We then cooled the CIMM to its base temperature and then incrementally decreased the voltage biases while measuring the resulting current. The results are shown in Fig. 5. A total of 30 bolometers were electrically connected, and we successfully operated 28. There are broad stable regions on many channels. Several channels become unstable at high fractional resistance, and we suspect that this is due to a mismatch between the detector and electrical bandwidths, rather than instability due to parasitic impedance. The residual resistance measured after the detector is superconducting [10, 19] contributes to crosstalk and detector instability at low operating resistance. The measured values have a median of $60 \text{ m}\Omega$, which is a reduction by about a factor of five compared to currently deployed systems.

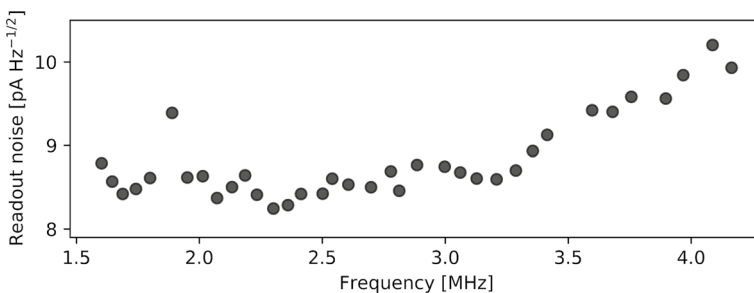


Fig. 4 Measured readout noise as a function of bias frequency for 36 channels. The median value is $8.6 \text{ pA/Hz}^{1/2}$. The slight increase in noise with frequency is likely due to an effect related to the SQUID feedback [6] and is suppressed significantly compared to deployed instruments

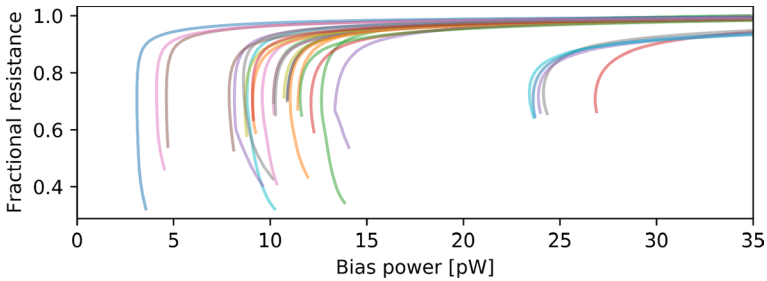


Fig. 5 (Color figure online) A set of TES bolometers are cooled through their superconducting transition by lowering the applied voltage biases. The TES bolometers used had varied normal resistance and saturation power

4 Conclusions

We have demonstrated several improvements to TES multiplexing using DfMux readout, including a substantial reduction in readout noise and operation of many TES bolometers under an inductive bias. The reduction in readout noise is a crucial step toward future applications of DfMux readout. The noise reduction was achieved by operating the SQUID array at lower temperature and with low dynamic impedance tuning. Additionally, parasitic impedances which are known to affect the frequency dependence on the readout noise have been significantly reduced by the circuit board design. The decrease in residual superconducting resistance in the TES bias circuit will allow for TES operation at lower resistance, resulting in higher responsivity and a further suppression of readout noise compared to deployed CMB DfMux systems. The improvements made to the cryogenic architecture significantly relax the constraints on the cryogenic cables, making the cryogenic packaging more robust and much simpler to procure. We are developing a version of the CIMM that is compatible with the POLARBEAR-2 receivers, and we hope to deploy several CIMM modules in the near future. The datasets generated during and/or analyzed during the current study are available from the corresponding author on reasonable request.

Acknowledgements This work was supported by Early Career Research Program, Office of Science, of the U.S. Department of Energy. Many of the figures were made using Matplotlib [20] and PGF/TikZ [21]. Analyses were conducted using Python scientific packages [22, 23].


Open Access This article is licensed under a Creative Commons Attribution 4.0 International License, which permits use, sharing, adaptation, distribution and reproduction in any medium or format, as long as you give appropriate credit to the original author(s) and the source, provide a link to the Creative Commons licence, and indicate if changes were made. The images or other third party material in this article are included in the article's Creative Commons licence, unless indicated otherwise in a credit line to the material. If material is not included in the article's Creative Commons licence and your intended use is not permitted by statutory regulation or exceeds the permitted use, you will need to obtain permission directly from the copyright holder. To view a copy of this licence, visit <http://creativecommons.org/licenses/by/4.0/>.

References

1. M.A. Dobbs et al., Frequency multiplexed superconducting quantum interference device readout of large bolometer arrays for cosmic microwave background measurements. *Rev. Sci. Instrum.* **83**(7), 073113 (2012). <https://doi.org/10.1063/1.4737629>
2. A.N. Bender et al., Digital frequency domain multiplexing readout electronics for the next generation of millimeter telescopes. in *Proceedings SPIE* **9153**, 91531A (2014). <https://doi.org/10.1117/12.2054949>
3. L. Gottardi et al., Development of the superconducting detectors and read-out for the X-IFU instrument on board of the X-ray observatory Athena. *Nucl. Instrum. Methods Phys. Res. A* **824**, 622–625 (2016). <https://doi.org/10.1016/j.nima.2015.09.072>
4. K. Rotermund et al., Planar lithographed superconducting LC resonators for frequency-domain multiplexed readout systems. *J. Low Temp. Phys.* **184**(1–2), 486–491 (2016). <https://doi.org/10.1007/s10909-016-1554-4>
5. T. de Haan et al., Improved performance of TES bolometers using digital feedback. in *Proceedings SPIE* vol 8452, 84520E (2012). <https://doi.org/10.1117/12.925658>
6. A.N. Bender et al., Year two instrument status of the SPT-3G cosmic microwave background receiver. in *Proceedings SPIE* vol 10708 <https://doi.org/10.1117/12.925658>
7. M. Hazumi et al., LiteBIRD satellite: JAXA's new strategic L-class mission for all-sky surveys of cosmic microwave background polarization. in *Proceedings SPIE* vol 11443, p. 114432F <https://doi.org/10.1117/12.2563050>
8. T. de Haan et al., Recent advances in frequency multiplexed TES readout: vastly reduced parasitics and an increase in multiplexing factor with sub-kelvin SQUIDs. *J. Low Temp. Phys.* **199**(3–4), 754–761 (2020). <https://doi.org/10.1007/s10909-020-02403-8>
9. A.E. Lowitz et al., Performance of a low-parasitic frequency-domain multiplexing readout. *J. Low Temp. Phys.* **199**, 192–199 (2020). <https://doi.org/10.1007/s10909-020-02384-8>
10. T. Elleflot et al., Effect of stray impedance in frequency-division multiplexed readout of TES sensors in POLARBEAR-2b. *J. Low Temp. Phys.* **199**(3–4), 840–848 (2020). <https://doi.org/10.1007/s10909-020-02387-5>
11. J. Montgomery et al., Performance and characterization of the SPT-3G digital frequency multiplexed readout system using an improved noise and crosstalk model. in *Proceedings SPIE* vol 11453, p. 014001 (2020). <https://doi.org/10.1117/12.2561537>
12. J.S. Avva et al., Design and assembly of SPT-3G cold readout hardware. *J. Low Temp. Phys.* **193**(3–4), 547–555 (2018). <https://doi.org/10.1007/s10909-018-1965-5>
13. M. Silva-Feaver et al., Comparison of NIST SA13a and SA4b SQUID array amplifiers. *J. Low Temp. Phys.* **193**(3–4), 600–610 (2018). <https://doi.org/10.1007/s10909-018-2052-7>
14. J. van der Kuur et al., Progress on Frequency-Domain Multiplexing Development for High Count rate X-ray Microcalorimeters. in *AIP Conference Proceedings* vol 1185, pp. 245–248 (2009). <https://doi.org/10.1063/1.3292324>
15. M.D. Audley et al., SQUID noise in a 176-pixel FDM demonstrator for the SAFARI far-infrared spectrometer. *J. Low Temp. Phys.* **199**(3–4), 723–729 (2020). <https://doi.org/10.1007/s10909-020-02399-1>
16. J. Clarke, A. Braginski, *The SQUID Handbook* (John Wiley Sons, Hoboken, 2004)
17. B. Westbrook et al., Detector fabrication development for the LiteBIRD satellite mission. *Proceedings SPIE* vol 11443, p. 114435Q (2020). <https://doi.org/10.1117/12.2562978>
18. T. Matsumura et al., LiteBIRD: Mission overview and focal plane layout. *J. Low Temp. Phys.* **184**(3–4), 824–831 (2016). <https://doi.org/10.1007/s10909-016-1542-8>
19. T. Elleflot et al., Detector and readout assembly and characterization for the simons array. *J. Low Temp. Phys.* **193**(5–6), 1094–1102 (2018). <https://doi.org/10.1007/s10909-018-2058-1>
20. J.D. Hunter, Matplotlib: A 2D Graphics environment. *Comput. Sci. Eng.* **9**(3), 90–95 (2007). <https://doi.org/10.1109/MCSE.2007.55>
21. T. Tantau. *The TikZ and PGF Packages: Manual for version 3.0.0*
22. F. Perez, B.E. Granger, IPython: A system for interactive scientific computing. *Comput. Sci. Eng.* **9**(3), 21–29 (2007). <https://doi.org/10.1109/MCSE.2007.53>
23. S. van der Walt et al., The numPy array: a structure for efficient numerical computation. *Comput. Sci. Eng.* **13**(2), 22–30 (2011). <https://doi.org/10.1109/MCSE.2011.37>

Publisher's Note Springer Nature remains neutral with regard to jurisdictional claims in published maps and institutional affiliations.

Authors and Affiliations

T. Elleflot¹  · **A. Suzuki**¹ · **K. Arnold**² · **C. Bebek**¹ · **R. H. Cantor**³ · **K. T. Crowley**⁴ · **J. Groh**⁵ · **T. de Haan**⁶ · **A. Hornsby**⁴ · **J. Joseph**¹ · **A. T. Lee**^{1,4} · **T. Liu**⁷ · **J. Montgomery**⁸ · **M. Russell**² · **Q. Yu**⁴

¹ Lawrence Berkeley National Laboratory, Physics Division, Berkeley, CA 94720, USA

² Department of Physics, University of California San Diego, San Diego, CA 92093, USA

³ STAR Cryoelectronics, Santa Fe, NM 87508, USA

⁴ Department of Physics, University of California Berkeley, Berkeley, CA 94720, USA

⁵ National Institute of Standards and Technology, Boulder, CO 80305, USA

⁶ High Energy Accelerator Research Organization (KEK), Tsukuba, Ibaraki 305-0801, Japan

⁷ Electrical and Computer Engineering Department, Princeton University, Princeton, NJ 08540, USA

⁸ Physics Department, McGill University, Montreal, QC H3A 0G4, Canada